Mon. Not. R. Astron. Soc. **000**, 1–?? (2016) Printed 28 November 2016 (MN LaTeX style file v2.2)

Investigating overdensities around $z > 6$ galaxies through ALMA observations of [CII]

Tim B. Miller[1⋆], Scott C. Chapman[1], Christopher C. Hayward[2,3,4], Peter S. Behroozi[5]†, Matt Bradford[6,7], Chris J. Willott[8] and Jeff Wagg[9]

[1] *Department of Physics and Atmospheric Science, Dalhousie University, 6310 Coburg Road, Halifax, NS B3H 4R2, Canada*
[2] *Center for Computational Astrophysics, Flatiron Institute, 162 5th Avenue, New York, NY 10010, USA*
[3] *TAPIR 350-17, California Institute of Technology, 1200 E. California Boulevard, Pasadena, CA 91125, USA*
[4] *Harvard–Smithsonian Center for Astrophysics, 60 Garden Street, Cambridge, MA 02138, USA*
[5] *Department of Astronomy, University of California at Berkeley, Berkeley, CA 94720, USA*
[6] *California Institute of Technology, 1200 E. California Boulevard, Pasadena, CA 91125, USA*
[7] *Jet Propulsion Laboratory, 4800, Oak Grove Dr., Pasadena, CA 91109, USA*
[8] *NRC Herzeberg, 5071, West Saanich Rd, Victoira, BC V9E 2E7, Canada*
[9] *Square Kilometre Array Organization, Jodrell Bank Observatory, Lower Withington, Macclesfield, Cheshire SK11 9DL, UK Ran*

arXiv:1611.08552v1 [astro-ph.GA] 25 Nov 2016

Submitted

ABSTRACT

We present a search for companion [CII] emitters to known luminous sources at $6 < z < 6.5$ in deep ALMA observations. Our data is deep enough to detect sources down to $L_{[CII]} \sim 10^8$ at $z \sim 6$. We identify five robust line detections from a blind search of five deep fields centered on ultra-luminous infrared galaxies and QSOs, suggesting these objects may be highly biased tracers of mass in the early Universe. We find these companion lines to have comparable properties to other known galaxies at the same epoch. All companions lie less than 650 km s^{-1} and between 20–70 kpc (projected) from their central source, providing a constraint on their average halo masses of 1.4×10^{12} $M_\odot$. To place these discoveries in context, we employ a mock galaxy catalog to estimate the luminosity function for [CII] during reionization and compare to our observations. The simulations support this result by showing a similar level of elevated counts found around such luminous sources. Finally we explore the effects of these biased tracers on the measurement of the [CII] power spectrum for upcoming intensity mapping experiments.

Key words: cosmology: large-scale structure of Universe – galaxies: clusters: general – galaxies: groups: general – galaxies: high-redshift – galaxies: interactions – submillimeter: galaxies.

1 INTRODUCTION

In order to further our understanding of galaxy formation we must investigate how the first galaxies formed during the epoch of reionization (EoR). Recent gains in (sub)-millimetre interferometers has made it possible to detect galaxies out to redshift six and beyond both in continuum and spectroscopically (Maiolino et al. 2015; Riechers et al. 2013). This enables constraints on their physical properties such as star formation rate (SFR), dynamical mass and conditions in their ISM (inter-stellar medium) (Wang et al. 2013; Willott et al. 2015a,b). The most luminous galaxies found at $z > 6$ are expected to be highly biased tracers of the underlying dark matter, and will be expected to form in the most overdense regions of space. Hierarchical formation will cause these overdensities to grow with time, making it likely that these systems are progenitors of the most massive galaxies and structures we observe at any redshift. This makes observations of galaxies during the EoR a crucial probe of the early evolution of these massive systems. Observations of the most overdense systems during the EoR are key to constraining galaxy formation models

Previous attempts to measure the environments around extreme objects at high redshift have generally failed to find an excess of galaxies. Husband et al. (2013) attempt to detect Lyman Break Galaxies (LBGs) in the fields surrounding several z∼5 quasars. While they find tentative evidence for redshift clustering of LBGs around two of the quasars studied, they are not statistically over dense relative to the blank fields at these redshifts. Kim et al. (2009)

⋆ E-mail: tim.blake.miller@gmail.com
† Hubble Fellow

© 2016 RAS

search around five $z \sim 6$ QSOs for i-band dropouts by comparing $i-z$ color distributions to that of a blank field. They find both over-densities and under-densities of dropouts depending on the QSO field and conclude that that QSO's at z $>$ 6 may exist in rare and massive halos but the harsh radiation field could inhibit the formation of lower mass galaxies in their immediate vicinity. Similarly, Utsumi et al. (2010) search for LBGs around a z=6.43 quasar. They do not find any LBGs in the immediate vicinity ($<$ 2 Mpc) of the quasar but find 7 dropout-galaxies consistent with z∼6.5 at larger radius $\sim$ 3 Mpc, but again not statistically above the field density. They also suggest that this may be due to strong UV radiation from the quasar inhibiting galaxy formation even though it likely inhibits a massive halo. Generally quasars have not proved a fruitful avenue to sign-post galaxy proto-clusters at high redshifts, and previous studies seem to indicate a complex bias (e.g.,Trainor & Steidel (2012)).

Attempts have also been made to search for galaxy overdensities around the most distant sub-millimeter galaxies (SMGs). Most notably, HFLS3 has a redshift of 6.34 (Riechers et al. 2013), and is one of the most extreme objects known to exist during the EoR. HFLS3 appears to be a massive starburst with a SFR of ∼2900 $\mathrm{M}_\odot\ \mathrm{yr}^{-1}$, with gas and dust masses of 1×10^{11} $\mathrm{M}_\odot$ and 1.3×10^{9} $\mathrm{M}_\odot$ respectively. Following its discovery, two studies were conducted to search for an excess of galaxies (Laporte et al. 2015; Robson et al. 2014). Robson et al. followed up HFLS3 with SCUBA2 images at 450μm and 850μm wavelengths. They found no evidence for an excess of luminous sub-mm emitters (with implied $\mathrm{L}_{IR} > 5\times10^{12}$) on a scale of 1.5 Mpc around HFLS3. Laporte et al. used the *Gran Telescopio Canarias* (GTC) and the *Hubble Space Telescope* (HST) to search for an excess of Lyman-break galaxies (LBGs) in the same field. Even at the lower SFRs probed by the LBG technique, they do not find any significant evidence that HFLS3 is a member of a proto-cluster.

While these results appear somewhat at odds with expectations, the studies described above suffer due to sensitivity limits and shortcomings of the selection techniques used. Optical selection of LBGs is difficult during the EoR due to both the intrinsic faintness of galaxies at $z > 6$ and unknown contributions from dust extinction. Many galaxies at this redshift could have sufficiently large dust column densities to be highly obscured in the rest frame optical. Although sub-mm selection techniques avoid the problem of dust extinction the sensitivity limits from source confusion with single dish survey instruments like SCUBA2 mean that the many fainter galaxies that would be expected to trace such an over density will be too faint to detect.

Using deep observations with the Attacama Large Millimeter Array (ALMA) to detect dust continuum and ionized Carbon emission lines from galaxies in the EoR overcomes these problems. Carbon has one of the lowest ionization energies of the elements that are abundant in the early universe. Due to the fine structure of ionized Carbon, [CII], it is excited at 91K and then decays through the $^2P_{3/2} \rightarrow^2 P_{1/2}$ transition which emits a photon at 157.7 μm. [CII] is one of the brightest in star forming galaxies and is a major cooling mechanism in the ISM. Recent works have shown it is possible to study [CII] emission of high-redshift galaxies using ALMA. Capak et al. (2015) and Willott et al. (2015a) have studied the FIR and dust properties of galaxies using ALMA, while Willott et al. (2013) and Wang et al. (2013) have probed the [CII] and dust of the host galaxies of $z \sim 6$ Quasars.

A complementary method that can be used to probe galaxies during the EoR is intensity mapping. This method does not resolve individual galaxies but it has the advantage that it is sensitive to very faint sources. It produces a spatial power spectrum, which provides information about the distribution of emission sources. For [CII] the sources are galaxies and star forming regions. The 21 cm neutral hydrogen line and CO rotational lines are other emission lines that can be targeted for intensity mapping. The 21 cm lines traces the neutral IGM, which is useful for cosmology as it traces the matter distribution, where as the CO lines trace molecular gas. Gong et al. (2012) preform analytic calculations to predict the [CII] power spectrum at z$>$ 6. To reduce contamination from low redshift CO lines, they suggest a cross correlation study with the 21 cm line. These two lines are expected to be anti-correlated because the 21cm line traces neutral hydrogen and the [CII] line traces new stars, which are the source of ionizing photons. Silva et al. (2014) conduct a detailed study of low redshift CO contamination to [CII] intensity mapping and propose an experiment with high enough spatial resolution to mask CO sources and still extract a [CII] clustering signal. The TIME-Pilot experiment aims to make a measurement of the [CII] clustering signal at $5 < z < 9$ and will begin taking data in the near future (Hunacek et al. 2015; Crites et al. 2014). A direct study of [CII] emitters at $z > 6$ can help to inform these experiments.

In this paper, we investigate the hypothesis that the environments of extreme objects at $z > 6$ should possess an over density of galaxies with a sensitive search for [CII] emission lines. In § 2 we define our sample ALMA fields and develop a method to search for robust companion [CII] lines around previously observed extreme objects at $z \sim 6$. In § 3 we describe the results of a similar analysis preformed on a simulated galaxy sample from the Hayward et al. (2013) (H13) mock galaxy catalog. § 4 uses these observational and simulation results to describe the effect that biased regions of the $z > 6$ Universe could have on [CII] intensity mapping experiments. Finally the results as a whole are discussed and summarized in § 5 and § 6 respectively. Throughout this study we assume a ΛCDM cosmology with parameters of h= 0.7 Mpc^{-1}, $\Omega_\Lambda = 0.73$ and $\Omega_M = 0.27$.

2 ALMA OBSERVATIONS

2.1 Sample and Methods

Our sample consists of deep ∼ 1.2mm ALMA observations (Band-6) of five luminous objects at $z > 6$. We use our observations of two starbursts, CLM1 and WMH5 Willott et al. (2015b), two quasars CFHQSJ0210-0546 and J2329-0301 Willott et al. (2013), as well as the data retrieved from the archive an additional quasar J054-0005 from Wang et al. (2013). For our 4 data cubes (Willott et al. (2013, 2015b)), we analyze the full ∼8 GHz from the four base bands, two centred on the extreme object, and two spaced $\sim$ 15 GHz away (in the upper sideband). In the archival data cubes (Wang et al. (2013)), we were only able to retrieve the 2 GHz baseband containing the quasar itself, and thus had less continuum sensitivity and frequency bandwidth to search for companions. All these data were obtained between 2012 and 2014, and we refer the reader to the papers cited for full context on calibrations, reductions and observing strategies. The depths of these observations vary by a factor $\sim$ 2 (listed in Table 1), but are deep enough to detect sources down to typically $\mathrm{L}_{[CII]} \sim 10^8\ \mathrm{L}_\odot$ at $z \sim 6$, probing a new regime to search for companion galaxies to these extreme objects. Describe cubes used and give references to old papers

To search for line candidates in the ALMA data cubes, we developed a blind search algorithm. First the entire cube was searched

Table 1. Properties of fields searched for companions

Source Targeted	Frequency Coverage (GHz)	RMS Noise* (mJy)	Reference
CLM-1	249.3 - 252.9 , 264.3 - 267.9	0.18	Willott et al. (2015b)
WMH-5	253.0 - 256.8 , 268.0 - 271.8	0.22	Willott et al. (2015b)
J0210-0456	254.7 - 256.2	0.34	Willott et al. (2013)
J2329-0301	255.4 - 257.1	0.25	Willott et al. (2013)
J2054-0005	269.2 - 270.9	0.38	Wang et al. (2013)

*Per 15 MHz channel

to find all points in the cube which displayed a flux greater than $3\times$ the rms noise in a single 15 MHz channel (typically 0.7 mJy beam^{-1}). With these positions recorded the same positions in neighbouring frequency slices were searched. If four surrounding channels (a minimal physical line width of ~ 50km s^{-1}) had fluxes greater than $2\times$ the rms noise (typically 0.5 mJy beam^{-1}), the source was deemed a possible line candidate. The significance of these candidates was then investigated. The FWHM of the candidate was measured by fitting a Gaussian, and channel maps of this FWHM were constructed around each candidate. The signal to noise ratio (S/N) is calculated by dividing the integrated flux of the line by the average RMS of the surrounding channel maps. Any object with a S/N ratio greater then 4.7 is deemed a possible candidate. The possible candidates are then inspected by hand to ensure they show Gaussian-like line profiles. The five objects which were identified by the algorithm to found to have S/N ratios greater then 4.7 and show Gaussian line profiles are deemed likely real lines and presented in the results section below. To further test the algorithm, we lowered the S/N cutoff to 4, identifying a further 15 candidates. These objects generally displayed lower FHWM and peak fluxes than the $> 4.7\sigma$ sources. We ran additional tests on the full sample of $> 4\sigma$ lines to test for their purity, as described in the subsection below.

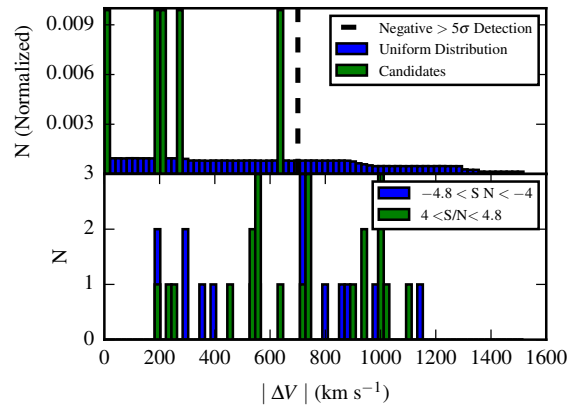

Figure 1. (Top) This panel displays the projected velocity offsets of the candidates from the central galaxies as well as the expected distribution if the candidates were uniformly distributed in the data cubes. Through a Monte Carlo analysis we find that the candidates are biased to a lower ΔV with respect to the uniform distribution at a 2σ significance level. **(Bottom)** This panel displays the velocity distribution, relative to the central source, of positive and negative candidates with $4 <$ S/N < 4.8. They appear to have a more uniform distribution, unlike the S/N > 5 candidates which appear to be biased to lower velocities

2.1.1 Purity of sample

Although our line candidates typically display a S/N > 5 it is still possible that they could be spurious due to the non-gaussian phase noise from the interferometer, and the large number of independent beams in the data cubes. To estimate the rate at which false positives could occur, we apply our search algorithm to find negative peaks in the data. At a S/N < 4.5, we find negative peaks, at the same S/N have similar distributions and properties to positive peaks, small FWHM values, likely unphysical given their fluxes. However there was only one negative peak with S/N> 5 (in the CLM1 cube). This could naively imply that 1 of the 5 robust line candidates is a false positive. A similar search for [CII] emitters in an ALMA deep field was performed by Aravena et al. (2016) Their observations are not quite as deep as the data we present here, however they use eight frequency tunings, covering the frequency range 212.0–272.0 GHz, and thus have $8\times$ more independent beams per pointing than our study, and must be even more cautious of false positives in a blind search. By contrast with our study, they find many negative line peaks even at $> 5\sigma$ significance, and estimate that at least half of their sample, and up to 90% of the lines are likely spurious detections. Figure 1 displays the distribution of the velocity offset between the candidates and the central galaxies as well the expected distribution if the candidates were uniformly distributed in the data cubes. The sidebands for the CLM-1 and WMH-5 cubes, as shown in 1, are not shown in Fig. 1 as the velocity offset reach $> 10,000$ km s^{-1} and is difficult to show along with the smaller offsets. It appears that the candidates do not trace the expected distribution and are biased towards being closer to the central galaxies. This would reinforce the idea that the candidates are real galaxies that are physically associated with the central galaxies. To test this we perform a Monte Carlo analysis by repeatedly sampling 5 elements from the expected distribution and calculate the probability that all 5 elements have a lower ΔV than the maximum of the candidates (642 km/s for CLM1-A). This calculation includes the sidebands for the CLM-1 and WMH-5 cubes that are not shown in Fig.1. After 10,000 iterations we find that 99% of them contain at least 1 of the randomly selected ΔV that is larger than the maximum of the candidates. Although this is only a marginal statistical detection ($\sim 2.5\sigma$), it is consistent with the candidates more likely appearing closer to the central galaxies with respect to a uniform distribution in the data cubes. As the velocity offset of CLM1-A (642 km s^{-1}) is significantly larger then the next highest candidate (J2054-0005-A at 278 km s^{-1}) we also investigate the likelihood to find 4 candidates withing 278 km s^{-1}. This is even less likely with $> 99.9\%$ of iterations contain at least 1 of 4 candidates that is larger then 278 km s^{-1}, a $\sim 4\sigma$ detection. Our Monte Carlo analysis of the velocity offset distribution supports the notion that we have uncovered real companion galaxies to the central sources as we find the candidates are biased to appear near the central galaxy.

Even if the sources are real we still must consider the possibility that these line are other transitions or species at different redshifts, The most likely being the mid-J CO transitions. The CO(3-2), CO(4-3) and CO(5-4) transitions are observable into the same

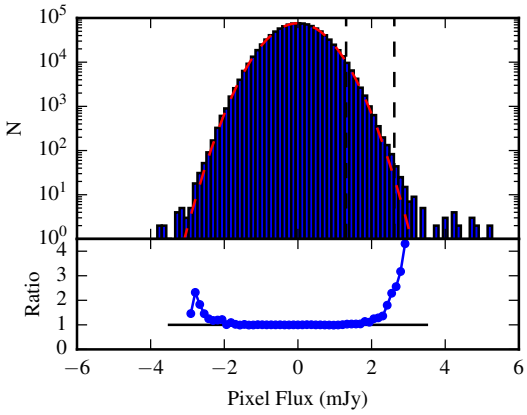

Figure 2. The top panel displays the distribution of voxel fluxes in the CLM-1 data cube. A Gaussian fit is shown in the red line. The ratio of the data to the Gaussian fit is displayed in the bottom panel. We see the distribution is well fit by a Gaussian over much of the distribution, except for at fluxes greater then 3 mJy. However, all these large positive pixel values can be attributed to detected sources. A excess of voxels is found in the $+2\sigma$ to $+4\sigma$ range, compared to the negative, however this is only observed in one of the other 4 cubes.

frequency band at approximate redshifts of 0.3, 0.8 and 1.2 respectively. Based on the Popping et al. (2016) models for the luminosity functions of CO emission, we naively expect to see ∼2 low redshift CO lines in the volume that our 5 cubes span. However we can rule out the possibility that our candidates are CO lines based on the width of the line. Table 2 shows the FWHM of our candidates, which are significantly smaller then what is observed for low redshift mid-J CO lines (typically FWHM > 250 km s^{-1} Iono et al. (2009); Daddi et al. (2014)). Combined with our Monte Carlo analysis of the ΔV distribution showing a non-uniform velocity distribution in the cube, we can rule out any significant contamination to our sample of candidates from low redshift mid-J CO lines.

2.1.2 Voxel Flux Distribution

To further examine the noise properties in our ALMA data cubes, we plot the distribution of voxel (data cube pixel) flux values for each field and show an example in Fig. 2 of the distribution of voxel fluxes in the CLM-1 cube, along with a Gaussian fit and the corresponding residuals. The distributions in each field are well represented by a Gaussian, showing residuals of less than 1 part in 50 for the - 3mJy to +3 mJy flux range. In the CLM-1 data cube, all fluxes at >3 mJy correspond to the detected sources. There is an excess of voxels in the $+2$ to $+4$ ×rms range compared to -2 to -4 ×rms, significant at the 3.6σ level. All other cubes display a similar distribution that is well fit with a Gaussian. However, only the J2054-005 cube shows a similar excess of voxels in the $+2$ to $+4$ ×rms range, here significant at the 2.8σ level. These excesses in the positive flux range reinforce our findings above with individually detected sources, possibly indicating the presence of a galaxy population below the adopted noise limits taken from our purity analysis. Further analysis on larger datasets will be required to confirm whether this can be attributed to the biased galaxy environments at $z > 6$ that our individual source analysis has suggested.

2.2 Results

Figure 3 displays the five line candidates found using our search algorithm on the ALMA datasets. showing the 1D spectrum, continuum and line maps for each candidate source. The channel map is extracted using the FWHM of the given line profile, while the continuum map is summed over the entire spectrum available. Contours on the continuum map show the detected line for comparison, revealing plausible continuum detection of 3 of the 5. A Gaussian function was fit to each line in order to extract a redshift as well as the integrated flux and FWHM of the line (Table 2). For the case of WMH5-B (Fig. 2e), there is contamination from the nearby primary source WMH5-A at frequencies lower than the line peak, and only the data at the peak and higher frequencies were used to fit the Gaussian line profile. The peak of the line is offset spatially by $0.7''$ from the peak of continuum emission, consistent with the bulk of this continuum coming from the brighter central source WMH5-A. Figure 6 in Willott et al. (2015b) displays a velocity offset vs position offset of these two sources, further illustrating that they are distinct galaxies.

Physical properties of the line candidates are listed in 2. All except for J2054-005-A have a S/N for the [CII] line of larger then five. Even though the S/N of J2054-005-A is not greater then 5, we consider it a robust detection as it displays a Gaussian like line profile and lies in close proximity to the central galaxy, J2054. There were several other possible line candidate with a similar SNR to J2054-A (4.5<S/N<5). However these possible line candidates were often at a large distance from the primary beam, $>$ 18 $''$ from the center, making them more likely to be due to noise or displayed non-realistic line profiles. This includes not showing a smooth Gaussian profile and having unrealistically low FWHM values for galaxies at this epoch (FHWM $<$ 60 km s^{-1}) . The FWHM values range from 75 to 189 km s^{-1}, and the $L_{[CII]}$ range from 7×10^7 $L_\odot$ to 2.5×10^8 $L_\odot$ (corresponding to a range of integrated line fluxes of 0.07 – 0.25 Jy km s^{-1}). This data is displayed in Fig. 4. Our FHWM/luminosity values are reasonable for physical galaxies, assuming typical mass/SFR estimates for galaxies at this epoch (e.g., Capak et al. (2015)). Continuum detection would provide a further test of the likely reality of our companions. Three of our line candidates do not have significant ($> 3\sigma$) continuum detections, although there is a positive $\sim 1.5\sigma$ excess at the position of all lines. As discussed, the continuum is difficult to measure for WMH5-B due to the proximate brighter primary source, however there is no doubt to the reality of the line detection here (and as discussed in Willott et al. (2015b)).

Our line candidates and primary galaxies are compared to [CII] detections of $z \sim 5$ LBGs in Capak et al. (2015) in figure 4 where the [CII] FWHM vs $L_{[CII]}$ is plotted for our candidates and their central brighter sources. The dotted line shows, based on our algorithm, the minimum luminosity needed to reach a SNR of 5 for each FWHM value. This assumes a Gaussian line profile and a typical noise of our cubes (RMS∼0.25 mJy). Our candidates follow a similar distribution to the Capak et al. galaxies, extending an apparent relation to slightly lower $L_{[CII]}$ and FWHM. The fact that none of the candidates appear as outliers in this distribution supports our findings above of high purity and low chances of false positives.

Taking our five candidates as real galaxies, we can work out the luminosity densities represented by our fields. To calculate the volume of space searched for candidates we then need an angular area on the sky and a redshift range for each field. We assume the area on sky searched includes the ALMA primary beam (a circle

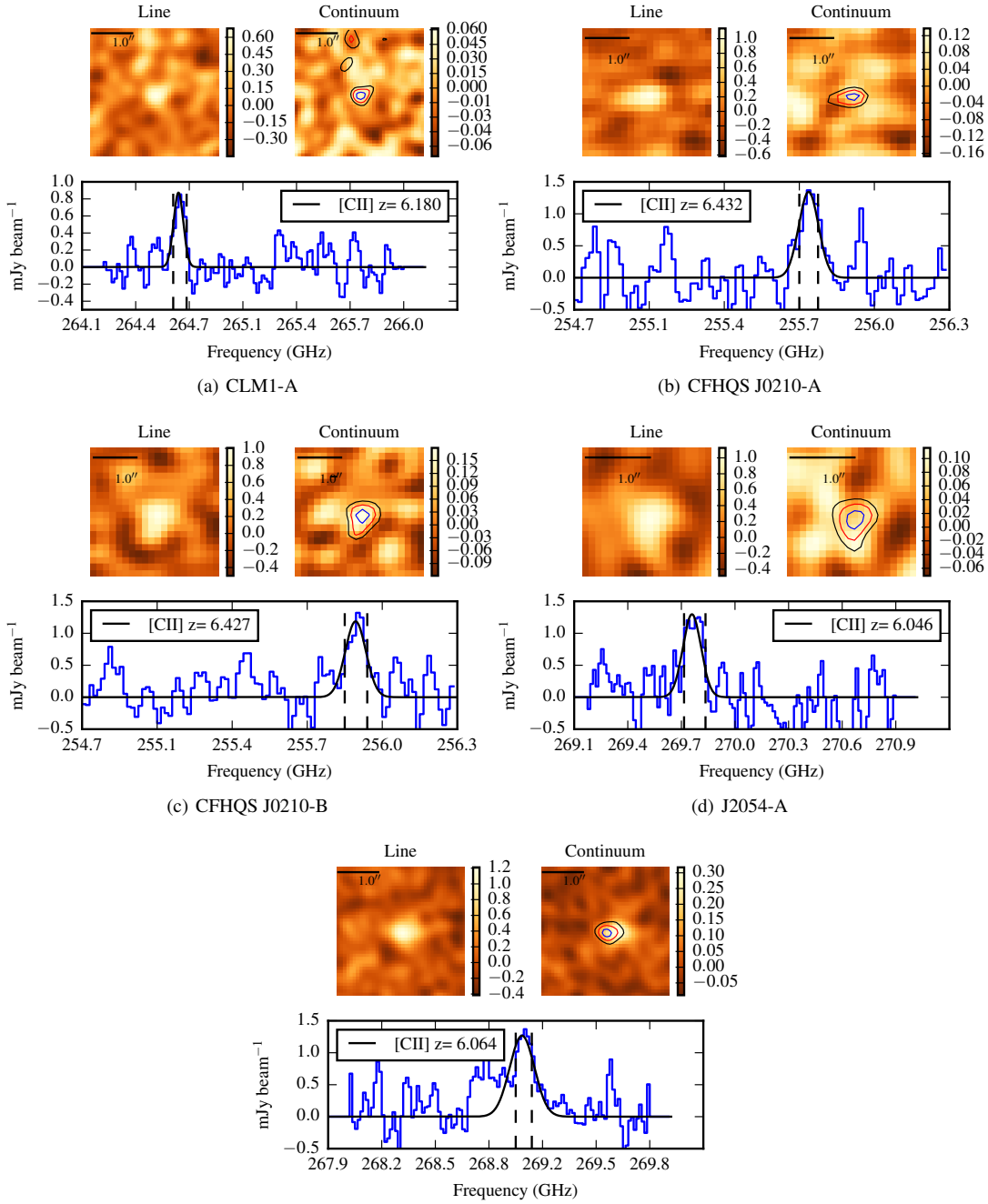

(a) CLM1-A

(b) CFHQS J0210-A

(c) CFHQS J0210-B

(d) J2054-A

(e) WMH5-B

Figure 3. The five line candidates found by the blind search of the deep ALMA cubes are shown here. Contours on the continuum images represent 0.9, 0.7 and 0.5 times the peak flux in the corresponding line channel. a) A candidate found near the UV luminous LBG CLM1. ALMA data was originally taken by and analyzed in Willott et al. (2015b). b) A candidate found near the Quasar J0210-0456, originally analyzed by Willott et al. (2013). c) A candidate found near the quasar J2054-0005. The ALMA data of the quasar was taken and analyzed in Wang et al. (2013). d) A candidate found near the source WMH5, also analyzed in Willott et al. (2015b). They point out the source and ackowledge it is likely a smaller galaxy undergoing a merger with the central source. We make an effort to fit the line profile separately.

with r = 12 $''$), except for the J2054 field where the candidate is found just outside of the primary beam ($\sim 14.5\,''$ from the center). For this field the a circle with an angular radius equal to that of the candidate is assumed to be searched. The redshift range searched is found through the spectral coverage of the ALMA data cubes, found in Table 1, and the known rest frame emission of the [CII] line at 157.7 μm

Figure 5 displays the estimates for the luminosity function (LF) of [CII] emitters at high redshift from our study, as well as other recent measurements and predictions. Our data is shown for just the companion galaxies, and also with both the companions and their central primary galaxies. Where we have only one galaxy at $> 10^9$ L$_\odot$, we treat our data as an upper limit. It is clear that our measurements are all well above all the previous measurements and

Table 2. Displaying properties of 5 line candidates. found by using the blind search algorithm described above.

Source Name	CLM1-A	CFHQSJ0210-0546-A	CFHQSJ0210-0546-B	WMH5-B	J2054-005-A
RA (J200)	2:25:02.970	2:10:13.883	2:10:13.501	2:26:27:0.25	20:54:06.66
DEC (J200)	-4:16:11.74	-4:56:22.86	-4:56:19.26	-4:52:38.38	-0:05:26.00
Peak Flux (mJy)	0.861	1.19	1.320	1.37	1.20
Integrated Line Flux (Jy km s^{-1})	0.07 ± 0.01	0.16 ± 0.03	0.15 ± 0.03	0.25 ± 0.04	0.19 ± 0.03
FWHM (km s^{-1})	75 ± 14	113 ± 22	118 ± 24	189 ± 45	137 ± 27
$L_{[CII]}$ (10^8 $L_\odot$)	0.7 ± 0.2	1.8 ± 0.5	1.6 ± 0.4	2.5 ± 0.5	1.9 ± 0.5
Line SNR	5.01	5.12	5.04	8.3	4.78
Continuum SNR	1.73	1.44	3.22	6.9	1.23
Estimated mass of central halo ($\mathrm{Log}_{10}(M_\odot)$)	$13.6^{+0.2}_{-0.3}$	< 12.4	$12.4^{+0.5}_{-1.2}$	$12.4^{+0.5}_{-1.3}$	$13.0^{+0.4}_{-0.7}$

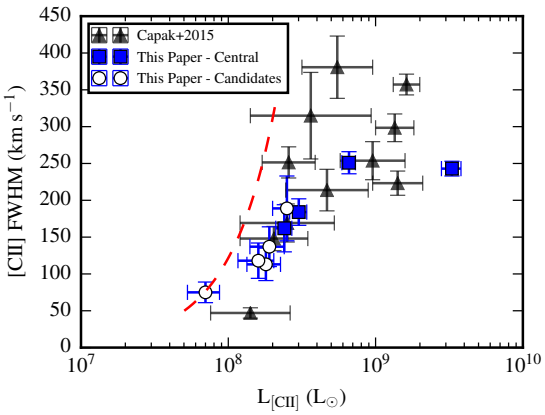

Figure 4. This figure displays our line candidates compared to the Capak et al. (2015) sample of $z \sim 5$ LBGs in the [CII] FWHM vs $L_{[CII]}$ plane. The red line shows for any FWHM value the minimum luminosity needed to achieve a SNR of 5. This is based on a Gaussian line profile and typical noise in our cubes (RMS∼0.25 mJy). Our line candidates and primary galaxies follow a similar distribution to the Capak et al. galaxies, with our candidate companions extending an apparent relation to slightly lower $L_{[CII]}$ and FWHM. The fact that none of the candidates appear as outliers in this distribution supports their reality.

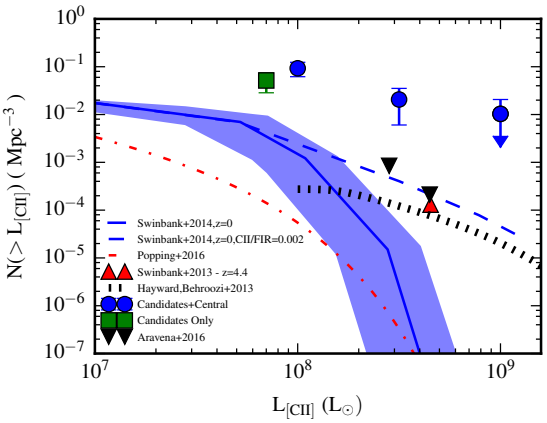

Figure 5. This plot displays various measurements and predictions for the luminosity function of [CII] emitters at z=6.The blue points represents the previously studied galaxies from our cubes and the line candidates described in Table 2. The downward blue triangle represents an upper limit as we only have 1 galaxy at the luminosity. The green square represents solely the density line candidates The black points show recent observational constraints made be Aravena et al. (2016) at $6 < z < 8$ and the red triangle shows a measurement by Swinbank et al. (2012) at $z = 4.4$. The blue shaded area shows a prediction by Swinbank et al. (2014) based on the local IR luminosity function taking into account observed fluctuations in the L_{IR} to $L_{[CII]}$ relationship while the dotted blue line assumes a constant $L_{[CII]}/L_{IR}$ of 0.002. A prediction from Popping et al. (2016) for the $z = 6$ [CII] luminosity function based on semi-analytical models is also shown. only. Hayward et al. (2013) displays a prediction from an abundance matching model combined with the empirical SFR-$L_{[CII]}$ relation from Pineda et al. (2014). Section 3 contains a full description of the Hayward et al. model.

predictions or estimations, although the state of the constraints at $z > 4$ are still very poor. The most constraining *field* measurement comes from the deep band-6 ALMA blank field from Aravena et al. (2016), which was searched for [CII] at the positions of optical drop outs. A measurement of the [CII] LF at $z \sim 4.4$ derived from two serendipitous [CII] detections by Swinbank et al. (2012). Popping et al. (2016) combine semi-analyticgalaxy formation models with radiative transfer calculations to predict CO and CII LFs at $z = 6$. A prediction for the [CII] LF based on the local IR LF (Sanders et al. 2003), taking into account variations in the $L_{[CII]}/L_{IR}$ relation. A similar calculation is also shown except assuming a fixed $L_{[CII]}/L_{IR}$ of 0.002. The Hayward et al. (2013) prediction comes from a dark matter only simulation, where SFRs are assigned to halos based on abundance matching. $L_{[CII]}$ is the assigned based on the empirical SFR-$L_{[CII]}$ relation derived in Pineda et al. (2014). A full description of this method is shown in Section 3.

We expect our sample is extremely biased given we searched around some of the most extreme galaxies known in the $z > 6$ Universe, and it is not surprising to find our points are all more than an order of magnitude above previous limits. Even just our companion galaxies on their own lie almost an order of magnitude above the highest measurements and predictions for the $L_{[CII]}$ luminosity function, demonstrating that these are biased fields and not just chance detections of unassociated field galaxies. We find an overdensity of $L_{[CII]} > 10^8$ of ~ 10 around QSOs and ULIRGs at $z > 6$.

We can also use these detected companions to constrain the halo masses in which they reside. We estimate the dynamical masses of the haloes by using the projected velocity and separation between the companion and central source in each field. With the assumption that these motions are virial, and have relaxed into a single potential, we can fit a theoretical line of sight velocity dis-

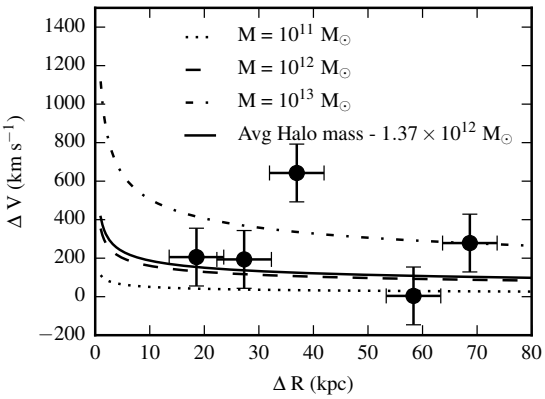

Figure 6. The projected velocity vs projected spatial offset between the candidates and central galaxies is plotted. The lines shows the expected velocity dispersion as a function of projected distance and halo mass. This profile is derived in Lokas & Mamon (2001) and we follow the same implementation as Swinbank et al. (2006) who preform this calculation on SMGs. The derived halos masses from this method are found in Table 2 with the velocity dispersion profile for the mean halo mass of 2.92 $\times 10^{12}$ M$_\odot$ is also plotted here.

persion profile to the velocity and spatial offset of the candidates. The only free parameter will be the dynamical mass of the central galaxy. The model for the line of sight velocity dispersion profile is derived in Lokas & Mamon (2001). Assuming a NFW halo profile, the radial velocity dispersion (σ_r) is found by solving the Jean's equation. Then following Binney & Mamon (1982) the line of sight velocity dispersion (σ_{LOS}) for a spherical non-rotating system is found by numerically integrating the following expression.

$$\sigma^2_{LOS}(R) = \frac{2}{\Sigma_M(R)} \int_R^\infty (1 - \beta \frac{R^2}{r^2}) \frac{\rho \sigma_r^2(r,\beta) r}{\sqrt{r^2 - R^2}} dr \quad (1)$$

where R is the projected radius, $\Sigma_M(R)$ is the surface mass density, obtained by integrating the density along the line of sight. β is a measure of the anisotropy of the velocity dispersion. We will take the limit where $\beta = 1$ (which assumes no anisotropy in the orbits). This is the same as assuming $\sigma_r \gg \sigma_\theta$, that the velocity dispersion is much larger in the radial than the azimuthal direction. There are caveats to this calculation which arise from the fact that the virial theorem is being applied to a merging system that is inherently not in equilibrium. Swinbank et al. (2006), who preform this calculation for $1.3 < z < 2.5$ SMGs, contains a detailed discussion of the caveats when this model is applied to merging galaxies.

Similar to Swinbank et al. (2006) we assume a concentration parameter (c) of 7 and a virial radius (R_{vir}) of 200 kpc. Figure 6 displays the projected velocity and spatial offset of the candidates as well as the expected velocity dispersion profile for 10^{11} M$_\odot$, 10^{12} M$_\odot$, 10^{13} M$_\odot$ halos and the mean derived dynamical mass of the central galaxy haloes of 1.37×10^{12} M$_\odot$. Note that each point represent a line candidate. Therefore the dynamical mass of CFHQS-J0210 will be measured twice since there are two candidates in the field. The estimated dynamical masses are shown in Table 2.

Table 2 shows the halos masses calculated from the velocity vs spatial offset analysis. Four of the candidates resulted in halo mass estimates while CFHQS J0210-B resulted in an upper limit for the CFHQS-J0210 halo mass. This upper limit is compatible with the estimate for the same halo from the other candidate CFHQS-J0210-A. The estimates halo masses range from just below $10^{12.4}$ M$_\odot$ to $10^{13.6}$ M$_\odot$, however the errors are quite large and often exceed an order of magnitude. Although the assumptions for c and R_{vir} are motivated based on typical values for massive galaxies (Mamon & Łokas (2005); Romanowsky et al. (2003)), to ensure it does not significantly affect the results, we repeat the calculation and vary what is assumed for c and R_{vir}. c was varied from 3 to 15 and R_{vir} from 100 kpc to 300 kpc. With a low R_{vir} of 100 kpc and a high c equal to 15, the estimated halo masses only increase by $\sim$ 0.2 dex. Similarly with a high R_{vir} of 300 kpc and a low c of 3, the estimated halo masses decrease by 0.3 dex. These were the most dramatic changes to the calculation when sampling different values for c and R_{vir}. Given the large measurement errors on the halo mass, the assumptions of c and R_{vir} are secondary uncertainties. Since we typically only have one object per halo our calculation represent a constraint and consistency check against other methods of estimating the dynamical mass. In order to truly measure the halo mass, more data points are needed to fit the profile opposed to using one and making assumptions about non-virial motions and anisotropies.

3 SIMULATIONS OF [CII] EMITTERS AROUND THE MOST LUMINOUS GALAXIES IN THE EOR

3.1 Mock Galaxy Catalogs

To interpret the results shown in Section 2 we employ a mock galaxy catalog described in Hayward et al. (2013), where we parametrize the galaxies primarily by their observed 850μm continuum. We provide a brief description of the methodology here but refer the reader to the original paper for full details. Using a halo catalog from the *Bolshoi* simulation 8 mock lightcones are constructed by starting at random locations and choosing a random sight line from $0.5 < z < 8$ (Klypin, Trujillo-Gomez, & Primack 2011; Behroozi et al. 2013b,c). Stellar masses and SFRs are assigned to halos based on their mass and redshift using the functions derived in Behroozi, Wechsler, & Conroy (2013a) from subhalo abundance matching. Dust masses and 850μm flux densities (S_{850}) are assigned based on Hayward et al. (2013). Dust masses are empirically assigned and a scaling function for S_{850} based on SFR and dust mass was derived by performing dust radiative transfer calculations on hydrodynamical simulations of galaxy mergers and isolated disk galaxies. We refer to SMGs in the catalog as any galaxy with an assigned $S_{850} > 3mJy$. We use these to represent bright sources during the EoR similar to the central sources described in section 2. We then assign [CII] luminosities to galaxies in the catalog based on the power law scaling with SFR empirically found in Pineda et al. (2014). We realize there are more sophisticated models for [CII] emission such as those described in Narayanan & Krumholz (2016). Their model considers galaxies as a collection of star forming clouds. Each cloud as several radial zones with differing temperature, chemical and ionization properties. From this they are able to calculate the [CII] luminosity for each cloud and therefore the entire galaxy.Although their method is physically motivated, since our sub-halo abundance matching model contains no detailed treatment of ISM micro-physics, we believe the empirical power law scaling with SFR is sufficient.

3.2 Simulation Results

The eight mock galaxy catalogs in total cover an area of 15.7 deg^2 extending out to $z = 8$ (1.4 $^\circ$ by 1.4° each field). In this area there

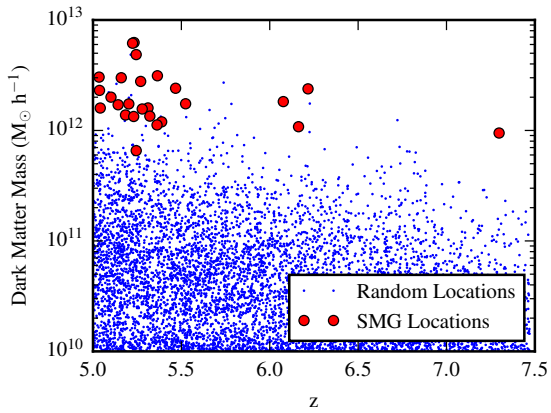

Figure 7. This figure display dark matter mass on the vertical axis and redshift on the horizontal axis. Dark matter mass is calculated by summing the mass of all the halos in a given region. The size of each region is 2 arcmin ^{2} with a redshift depth of 0.02. At this epoch the corresponding volume is approximately 100 Mpc^3. It is shown that SMGs consistently reside in the highest mass regions at this epoch.

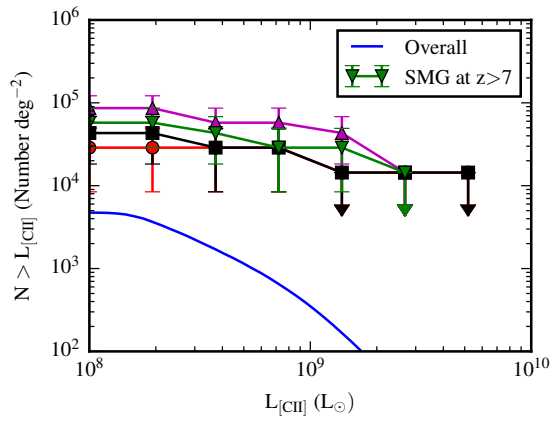

Figure 8. This plot shows the counts in the individual fields. The blue curve shows the average counts at this epoch and the other four colors represent the 4 regions that contain SMGS. Although there is some variation every field has higher counts at almost all luminosities. The downward arrows represent upper limits as there is only one galaxy in each field at that luminosity.

were four galaxies found at $z > 6$ (one at $z > 7$) during the epoch or reionization exhibiting extreme luminosities $L_{IR} > 10^{12}\,L_\odot$ ($S_{850\mu m} > 3$mJy). There are clearly many more SMGs at z<6, and our simulation reasonably represents the overall redshift distribution of SMGs found from observations, which peaks at z∼2.5 but has an extended tail out to $z \sim 6$ (Chapman et al. 2003; Simpson et al. 2014). Similar to our analysis of the central ALMA galaxies in § 2 we investigate how the SMG locations in the simulations signpost overdensities at $z > 6$. Given that we have full information available in the mock catalog, we are able to quantify how these biased regions around the most luminous SMGs trace the most massive overdensities during the EoR. First, to probe if SMGs represent peaks in large-scale structure at this epoch we compare the total mass of all dark matter halos in the biased regions compared to on average. Figure 7 shows the total dark matter mass in a 100 Mpc^3 cube around each SMG as well as many randomly located cubes. One can see that SMGs reside in the highest density regions, and especially at z>6. This reinforces the idea that luminous galaxies during EoR should signpost the most massive overdensites.

To investigate if SMGs present during reionization not only trace overdensities of matter but also galaxies, we show galaxy counts of fields centered at the known SMGs. The fields are $0.5' \times 0.5'$, comparable to the size of the ALMA fields (defined by their primary beams). Figure 8 shows the counts over the individual SMG-centered fields. We see that although there is some scatter, all the four biased fields show similar counts. It is noteworthy that each SMG field has at least one less luminous galaxy within a $\Delta z = 0.005$, similar to the central ALMA galaxies in §2, where four of the five fields searched contain a [CII] line candidate within the same redshift range. The biased fields in the simulation all converge to the same value at large [CII] luminosities as they all contain one ultra-luminous source in the same field size.

Figure 9 shows the total counts in the four fields surrounding the simulated $z > 6$ SMGs compared to that of the entire catalogue at $z > 6$. These SMGs have the highest SFRs in the entire catalog at these redshifts, and thus will have the highest $L_{[CII]}$, due to our adopted scaling relation. At $L_{[CII]} > 10^8\,L_\odot$, the counts in the SMG-centered fields are much higher then that of the field average, ranging from $\sim 10\times$ to $\sim 1000\times$ excesses. However, these four

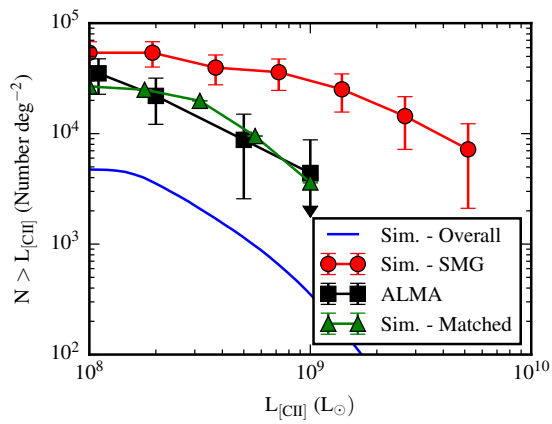

Figure 9. Here we show $L_{[CII]}$ galaxy counts comparing the 0.25 arcmin^2 regions surrounding the 4 SMGs in the simulation (red dots) to the entire catalog at z > 6 (blue line). We see that there are more galaxies in the SMG regions then on average at all luminosities. Error bars on this plot represent the Poisson counting uncertainty. Again the downward arrow represents an upper limit as there is only one galaxy in that field at the given luminosity. The black points are the results of counts of our line detection in the ALMA data described in § 2. The green points represent galaxies in the simulation with $L_{[CII]}$ matched to the central galaxies in § 2 ($L_{[CII]} = 3 \times 10^8 - 3 \times 10^9\,L_\odot$). We find very good agreement between the simulations and the observations.

simulated SMGs have much higher $L_{[CII]}$ than the central galaxies in our ALMA observations. To directly compare the simulations with our observed counts from our ALMA data, we take the fields surrounding simulated galaxies with $L_{[CII]}$ matched to that of the ALMA central galaxies($L_{[CII]} = 3 \times 10^8 - 3 \times 10^9\,L_\odot$) . Interestingly these *luminosity matched* simulated fields show a fairly good agreement with the counts in our ALMA observations, which provides some level of validation for the bias of galaxies to dark matter adopted in the simulation.

4 CII POWER SPECTURM

To preform analytic calculations on the spatial [CII] power spectrum during reionization ($P_{[\mathrm{CII}]}$) we will employ the Gong et al. model (described in Gong et al. (2012) and the references therein). Below is a brief description of the model and it's relevance to this work. To compute the power spectrum two separate terms are considered: the clustering power spectrum ($P^{clus}_{[\mathrm{CII}]}$) and the shot noise power spectrum ($P^{shot}_{[\mathrm{CII}]}$). The shot noise power spectrum is due to small number statistics, when the number of sources is small. This effect can be even further exaggerated when there is a single galaxy which is much more luminous than any others in the field. The total power spectrum is calculated below:

$$P_{[\mathrm{CII}]}(z,k) = P^{clus}_{[\mathrm{CII}]}(z,k) + P^{shot}_{[\mathrm{CII}]}(z) \tag{2}$$

The shot noise power spectrum dominates at high values of k (> 1 h Mpc^{-1}) where as the clustering power spectrum dominates at low values of k (< 0.1 h Mpc^{-1}). $P^{shot}_{[\mathrm{CII}]}$. The clustering power spectrum is calculated by rescaling the matter power spectrum.

$$P^{clus}_{[\mathrm{CII}]}(z,k) = \bar{b}^2_{[\mathrm{CII}]}\bar{I}^2_{[\mathrm{CII}]}P_{matter}(z,k) \tag{3}$$

$\bar{b}_{[\mathrm{CII}]}$ is the average galaxy bias weighted by CII luminosity, written as in Visbal & Loeb (2010). $\bar{I}_{[\mathrm{CII}]}$ is the mean intensity of the CII emission line. This is calculated in Gong et al. (2012) by employing a semi-analytical model described in De Lucia & Blaizot (2007). This model post processes the Millennium dark matter simulation to assign galaxy properties to halos.

Once we have the $\mathrm{L}_{[\mathrm{CII}]}$ counts we can quantitatively estimate the boost to the [C II] power spectrum during the epoch of reionization. One can show that the mean intensity is proportional to the integral shown below.

$$\bar{I}_{[\mathrm{CII}]} \propto \int L_{[\mathrm{CII}]}\frac{dN}{dL_{[\mathrm{CII}]}}dL_{[\mathrm{CII}]} \tag{4}$$

To compare the baised regions to the average, we take a simple numerical integral under both luminosity functions with respect to L_{CII} and then compute the ratio between the 2 regions. We then calculate the square of this ratio as the boost to the power spectrum as the clustering term is proportional to the mean intensity squared. Similarly the shot noise term can be written as follows (Uzgil et al. (2014)).

$$P^{shot}_{[\mathrm{CII}]} \propto \int L^2_{[\mathrm{CII}]}\frac{dN}{dL_{[\mathrm{CII}]}}dL_{[\mathrm{CII}]} \tag{5}$$

Using the number counts we have shown in Fig. 9 to calculate these integrals will not give the correct boost for most intensity mapping experiments as the surveys are often much larger than the $0.5' \times 0.5'$ regions we have used to compare to our ALMA data. To investigate we vary the size of the field used to calculate the $\mathrm{L}_{[CII]}$ luminosity function and thus the boost to each term of the power spectrum.

The results are shown in Figure 10. The boost to each term of the power spectrum from observing biased regions, traced by SMGs, to the entire field is shown on the vertical axis. The boost to the clustering terms comes from the ratio of the mean intensity squared (From Eqn. 4). The boost to the shot noise term is calculated as the ratio, between the biased regions and the entire field, of the integral shown in Eqn. 5. The horizontal axis displays the size of the field used to calculate the boost of the biased region. It is assumed that the survey is a square field centered at the position of the luminous galaxy. One can see that as the field size increases

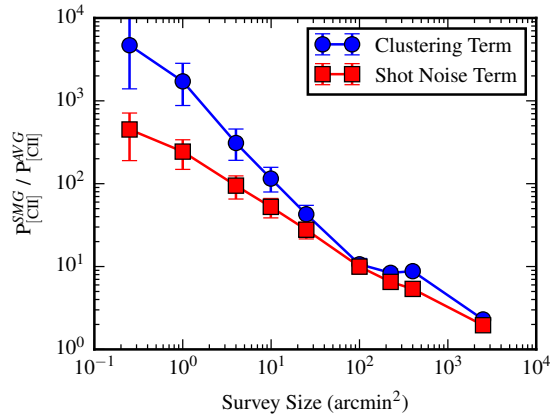

Figure 10. The boost to the power spectrum measured by observing a biased regions of space, as traced by SMGs, compared to that of the entire simulation is shown for different survey sizes. The blue circles show boost to the clustering power spectrum is calculated as the ratio of the mean intensities squared. The boost to the shot noise term,shown by the red squares, is the ratio of the integral in Eqn. 5. Although at small survey sizes, the boost to the clustering term is larger than the shot noise term, as survey size increases the clustering term decreases faster.

the boost to both the shot noise and the the clustering power spectrum, decreases. Although the boost to the clustering term is larger a low survey size, it decreases faster with a slope of -0.86. The shot noise term, in comparison, has a slope of -0.62.

The proposed TIME-pilot experiment will survey an area of 40 arcmin^2, however it will have a very elongated geometry of $80' \times 0.5'$. This is done to ensure the low-k modes of the power spectrum can be measured as there is one extended dimension. The geometry has a substantial effect on the boost to both terms on the power spectrum as it alters the luminosity function. The boost to a square survey of 40 arcmin^2 is 40 ± 10 and 27 ± 6 for the clustering and shot noise terms respectively. Comparatively for a survey with an elongated geometry, like TIME-pilot, the boost is 3 ± 0.8 and 6 ± 1 for the clustering and shot noise terms respectively. These boosts applied to the Gong et al. model for the $z = 6$ [CII] power spectrum are shown in Fig. 11.

For the TIME-pilot geometry, the boost to the power spectrum is about a order of magnitude smaller than a square survey. The shot noise term boost is about twice as large as the clustering term, leading to the boost being more evident in the high-k regime. The opposite is true in the square survey case. The clustering term boost is larger, therefore it is more noticeable in the low-k regime. The is shown in Figure 11.

5 DISCUSSION

We have searched deep ALMA data targeting [C II] from known $z > 6$ QSOs and ULIRGs. Our analysis has revealed 5 companion galaxies, one per field on average. The fact that the physical properties of our line candidates are comparable to those found by other ALMA studies targeted known high-redshift galaxies in [C II] (e.g., (Capak et al. 2015)) lends some confidence that most if not all of our sources are real, although the statistical analysis of the purity of our sample cautions that at least one of our candidates may be a false positive detection. However, as the faintest galaxy in our sample (CLM1-A) lies near our selecting limit (Fig. 4) and is somewhat low luminosity for its FWHM it may not be a real

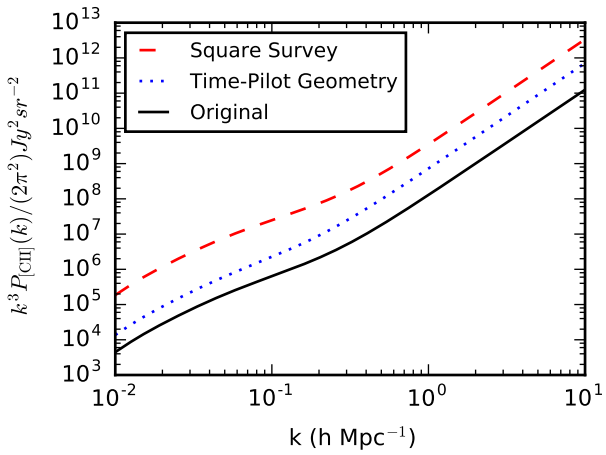

Figure 11. This figure shows the original Gong et al model at $z = 6$ as well as the boosted version if regions containing SMGs are observed. Both the blue and dotted red lines represent the boost if a 40 arcmin^2 region is observed with different geometries. The TIME-Pilot geometry (blue solid line) is $80' \times 0.5'$ rectangle, where as the square survey (red dotted line) is a $\sim 6' \times \sim 6'$ square field.

galaxy. However it is also possible that this galaxy is simply a relatively face on projection of a disk thus increasing it's true FWHM and easily matching the $L_{[CII]}$-FWHM relation.

We are able to robustly detect lower luminosity galaxies then other studies because the noise in these pointed deep fields is much lower then the larger area surveys. Aravena et al. (2016) perform a blind survey for $z > 6$ [CII] emitters in a blank field over a similar area (7 pointings covering ~ 1 arcmin^2), but a much larger volume due to their 7 frequency tunings over the ALMA band-6. However their average RMS of 0.56 mJy at 31.25 MHz channel^{-1} is about twice that of our fields. They find only $\sim 1-2$ line candidates which lie within the *physical* envelope of galaxies defined by our survey and that of Capak et al. (2015). They note specifically that for this reason, on top of their purity analysis, most of their candidates are probably not real. Despite the small angular size of our deep ALMA pointings, the biased regions have allow us to uncover lower luminosity galaxies than previously found due to their increased numbers in these over dense fields.

Recent works have found many $z > 6$ galaxies to have a large $L_{[CII]}$/ L_{IR} deficit (Willott et al. (2015a); Wang et al. (2013); Capak et al. (2015)). All these papers find systematically lower [CII] luminosities at a given L_{IR} when compared to $z < 3$ galaxies. This is often attributed to the lower dust-to-gas ratio at high redshift. The low IRX/β relation found by Capak et al. (2015) for their $5 < z < 6$ galaxies supports this argument. If true, this would suppress IR emission while the higher gas mass would enhance the [CII] emission. Other possible explanations include changes in the dust properties or lower metal abundances causing different UV spectral slopes. Capak et al. (2015) derive a metallicity of ~ 0.25 solar for their sample of galaxies from analyzing UV absorption features. The lack of significant continuum detections in the majority of our [CII] line candidates is consistent with the literature findings and and supports the hypothesis of a lower dust-to-gas ratio for these $z > 6$ galaxies. Obtaining deep rest frame UV and optical measurements of our ALMA fields will be an important followup to test the UV spectral slopes of our [CII] emitters.

Since our ALMA sample is biased to fields of extreme objects at $z > 6$, we are not able to directly constrain the field luminosity function, however we can make predictions about the clustering and bias of galaxies at this epoch (Fig. 5). Even if the existing blank field surveys were extended to deeper flux limits comparable to our fields, we predict based on our counts/overdensity analysis that these blank field surveys (e.g., Aravena et al. (2016)) would not be large enough to uncover significant numbers of fainter sources. By comparison to our simulations we find the number counts in regions surrounding galaxies with similar $L_{[CII]}$ to the central galaxies from the ALMA analysis show outstanding agreement to the observed data. We also note that the overall luminosity function from the simulations, shown in Fig. 5, shows fairly good agreement to observed estimates of the [CII] field luminosity function, although underestimate the observations slightly. This is remarkable for a simple power law $L_{[CII]}$ - SFR scaling relation combined with an abundance matching model. The factor $\sim 10\times$ over density we measure on average in the ALMA data is similar to what we find in fields of extreme galaxies in the simulation, and appears to reflect the true matter over density.

The simulations clearly have some limitations, and the apparent agreement with our ALMA observations should be measured with these caveats. In the mock galaxy catalogs, only star forming galaxies parameterized by their far-IR/sub-mm emission are adopted in this realization. The quasar-phase of galaxies and the growth of the super massive black holes is not specifically treated in this implementation. Thus the connection to our three QSO fields is not particularly well motivated, although the SMG and QSO phases have often been shown to be tightly linked (e.g., Harrison et al. (2012b,a)). We note that the mass of the halos that host SMGs in the simulation is similar to the estimated halo masses of z>6 quasars ($\bar{M}_{halo,SMG} \approx 5 \times 10^{11} M_\odot$, Wang et al. (2013)).

In a recent paper Miller et al. 2015 find that SMGs at $z \approx 2$, are actually fairly poor tracers of a majority of the most over dense regions and the most massive haloes, with many such regions displaying few if any SMGs. Generally, the simulated SMGs were shown to trace a large range of environments, from extremely overdense to significantly less dense then average, likely due to the stochasticity of their brief starburst phases, and small numbers relative to less luminous galaxies. Our work here represents an extension to higher redshifts of the analysis in Miller et al. 2015 , where our Fig. 7 shows that at $z > 5$ individual SMGs do begin to consistently trace the most massive regions at that epoch. At these high redshifts, all of the most massive galaxies that have formed are actively forming stars (none have been quenched), and the cosmic downsizing that is apparent in Miller et al. 2015 has not yet begun.

Although the boost to the clustering term of the power spectrum is tends to be larger then that of the shot noise term, the latter is likely more interesting and applicable for intensity mapping experiments. To measure the clustering term, which dominates at low k modes, the experiment must conduct contiguous coverage over large volumes. As shown in Fig. 10 the boost to both terms of the power spectrum drops significantly with increasing survey size. This make it fundamentally impossible to design an intensity mapping experiment to take advantage of the boost to the clustering term of the power spectrum. The shot noise term however is still accessible when surveying smaller areas since it dominates in the high k regime. Thus, we are able to take advantage of the boost to the shot noise power spectrum from pointing at known luminous objects.

The elongated geometry of the proposed TIME-pilot experiment presents a problem to obtain a large boost. For a field of the same size, the boost to the thin rectangle is about an order of

magnitude smaller than a square survey. The thin rectangle geometry means that only a small fraction of the overdensity is observed compared to a square. Therefore the contribution of the overdensity to the luminosity function is significantly smaller than the square survey case. However this effect is less pronounced for the shot noise term because it is largely dependent on a small numbers of luminous galaxies. As the sensitivity of these experiments improves there will be interesting applications of the boost. One is to constrain the bias of [CII] emitters at high redshift by measuring the power spectrum around luminous objects. We have shown in § 2 that luminous objects represent over densities at high redshift however with a full intensity mapping experiment it would be much easy to significantly increase the sample size. Although the TIME-pilot experiment is not ideal to capture the power spectrum boost due to the elongated geometry, there will be many application when the full TIME experiment and others arrive.

6 CONCLUSION

We present a successful search for companion [CII] emitters around known luminous sources during the EoR. Using ALMA to observe [CII] emission with ALMA allows us to overcome shortcomings of other similar studies trying to observe overdensities at z>6 around rare and extreme sources.

We develop an algorithm to search for companion [CII] line to deep band-6 ALMA data of previously observed luminous galaxies and quasars. A similar analysis is then preformed on a mock-galaxy catalog to put the ALMA results in context. The major results are as follows:

- We find 5 robust line candidates from our blind search of deep ALMA data of known luminous galaxies and quasars. All but one candidate display a [CII] line SNR of greater than 5, with the final one having a S/N of ~ 4.8 but exhibiting other properties of a real galaxy. All five candidates lie within a projected radius of 70 kpc and 600 km s^{-1} supporting the idea that they are physically associated to the central galaxies.
- The 5 candidates display similar physical properties to previously studied galaxies during the EoR. We find the same $L_{[CII]}$ vs. [CII] FWHM relation found in Capak et al. (2015) extended to lower luminosity values. Through analyzing projected separation vs. velocity offset of the candidates compared to the central galaxies we are able to constrain the central halo mass. We estimate an average halo mass of $1.37 \times 10^{12} M_{\odot}$.
- By calculating the luminosity function of the central galaxies and the candidates we quantify the over density. These luminous galaxies represent highly biased regions during the EoR. Even though there are few constraints on the luminosity function of [CII] emitters at $z > 6$ our fields show an overdensity of at least $\sim$10 compared to all models and measurements.
- By preforming a similar analysis on a mock galaxy catalog we find a comparable result to the ALMA observational analysis. The most luminous galaxies at $z > 6$ in the simulation represent overdense regions of [CII] emitters tracing peaks in the large scale structure. Matching the $L_{[CII]}$ of the extreme sources in the simulation to the central sources in our ALMA fields, we find a similar $\sim 10\times$ over density to the field population in our most luminous observed [CII] emitters.
- Looking forward to future intensity mapping experiments aimed at measuring the [CII] power spectrum during the EoR, we investigate the effect of observing these biased regions will have. Although with a square survey it is possible to boost the power spectrum by an order of magnitude or more, this will not be feasible with the TIME-pilot experiment. This is due to the elongated geometry which does not capture the entire overdensity in the survey.

ACKNOWLEDGEMENTS

TBM would like to thank the Killam Trust for support. SCC acknowledges the Killam Trust, NSERC and CFI for support. Support for PB through program number HST-HF2-51353.001-A was provided by NASA through a Hubble Fellowship grant from the Space Telescope Science Institute, which is operated by the Association of Universities for Research in Astronomy, Incorporated, under NASA contract NAS5-26555.

REFERENCES

Aravena M. et al., 2016, eprint arXiv:1607.06772
Behroozi P. S., Wechsler R. H., Conroy C., 2013a, ApJ, 770, 57
Behroozi P. S., Wechsler R. H., Wu H.-Y., 2013b, ApJ, 762, 109
Behroozi P. S., Wechsler R. H., Wu H.-Y., Busha M. T., Klypin A. A., Primack J. R., 2013c, ApJ, 763, 18
Binney J., Mamon G. A., 1982, Monthly Notices of the Royal Astronomical Society, 200, 361
Capak P. L. et al., 2015, Nature, 522, 455
Chapman S. C., Blain a. W., Ivison R. J., Smail I. R., 2003, Nature, 422, 695
Crites A. T. et al., 2014, in Proceedings of the SPIE, Holland W. S., Zmuidzinas J., eds., Vol. 9153, p. 91531W
Daddi E. et al., 2014, Astronomy & Astrophysics, 577, 46
De Lucia G., Blaizot J., 2007, Monthly Notices of the Royal Astronomical Society, 375, 2
Gong Y., Cooray A., Silva M., Santos M. G., Bock J., Bradford C. M., Zemcov M., 2012, The Astrophysical Journal, 745, 49
Harrison C. M. et al., 2012a, The Astrophysical Journal, 760, L15
Harrison C. M. et al., 2012b, Monthly Notices of the Royal Astronomical Society, 426, 1073
Hayward C. C., Behroozi P. S., Somerville R. S., Primack J. R., Moreno J., Wechsler R. H., 2013, Monthly Notices of the Royal Astronomical Society, 434, 2572
Hayward C. C., Narayanan D., Kereš D., Jonsson P., Hopkins P. F., Cox T. J., Hernquist L., 2013, MNRAS, 428, 2529
Hunacek J. et al., 2015, Journal of Low Temperature Physics
Husband K., Bremer M. N., Stanway E. R., Davies L. J. M., Lehnert M. D., Douglas L. S., 2013, Monthly Notices of the Royal Astronomical Society, 432, 2869
Iono D. et al., 2009, The Astrophysical Journal, 695, 1537
Kim S. et al., 2009, The Astrophysical Journal, 695, 809
Klypin A. A., Trujillo-Gomez S., Primack J., 2011, ApJ, 740, 102
Laporte N. et al., 2015, The Astrophysical Journal, 810, 130
Lokas E. L., Mamon G. A., 2001, Monthly Notices of the Royal Astronomical Society, 321, 155
Maiolino R. et al., 2015, Monthly Notices of the Royal Astronomical Society, 452, 54
Mamon G. A., Łokas E. L., 2005, Monthly Notices of the Royal Astronomical Society, 363, 705
Miller T. B., Hayward C. C., Chapman S. C., Behroozi P. S., 2015, Monthly Notices of the Royal Astronomical Society, 452, 878
Narayanan D., Krumholz M., 2016, 16
Pineda J. L., Langer W. D., Goldsmith P. F., 2014, Astronomy & Astrophysics, 570, A121

Popping G., van Kampen E., Decarli R., Spaans M., Somerville R. S., Trager S. C., 2016, 19
Riechers D. A. et al., 2013, Nature, 496, 329
Robson E. I. et al., 2014, The Astrophysical Journal, 793, 11
Romanowsky A. J., Douglas N. D., Arnaboldi M., Kuijken K., Merrifield M. R., Napolitano N. R., Capaccioli M., Freeman K. C., 2003, 1696
Sanders D. B. et al., 2003, The Astronomical Journal, 126, 1607
Silva M. B., Santos M. G., Cooray A., Gong Y., 2014
Simpson J. M. et al., 2014, The Astrophysical Journal, 788, 125
Swinbank A. M., Chapman S. C., Smail I., Lindner C., Borys C., Blain A. W., Ivison R. J., Lewis G. F., 2006, Monthly Notices of the Royal Astronomical Society, 371, 465
Swinbank A. M. et al., 2012, Monthly Notices of the Royal Astronomical Society, 427, 1066
Swinbank A. M. et al., 2014, Monthly Notices of the Royal Astronomical Society, 438, 1267
Trainor R. F., Steidel C. C., 2012, The Astrophysical Journal, 752, 39
Utsumi Y. et al., 2010, The Astrophysical Journal, 721, 1680
Uzgil B. D., Aguirre J. E., Bradford C. M., Lidz A., 2014, The Astrophysical Journal, 793, 116
Wang R. et al., 2013, The Astrophysical Journal, 773, 44
Willott C. J., Bergeron J., Omont A., 2015a, The Astrophysical Journal, 801, 123
Willott C. J., Carilli C. L., Wagg J., Wang R., 2015b, The Astrophysical Journal, 807, 180
Willott C. J., Omont A., Bergeron J., 2013, The Astrophysical Journal, 770, 13